Third International Conference on CFD in the Minerals and Process Industries
CSIRO, Melbourne, Australia
10-12 December 2003

THE EFFECT OF JET VELOCITY RATIO ON AERODYNAMICS OF RECTANGULAR SLOT-BURNERS IN TANGENTIALLY-FIRED FURNACES

S. AHMED, J. HART AND J. NASER

Cooperative Research Centre for Clean Power from Lignite
School of Engineering & Science, Swinburne University of Technology, Hawthorn, VIC-3122.

ABSTRACT

In a typical coal-fired power station boiler ignition and combustion of coal are largely controlled by burner aerodynamics, hence the geometry of the burner plays an important role in achieving stable combustion, high burnout of fuel, low production of pollutants and control of fouling. Current practice in pulverized coal fired boilers is to use either swirl burners or tangentially-fired slot-burners. The later system has been adopted for boilers in Victoria firing brown coal. To obtain a better understanding of the overall combustion process, it is important to investigate the aerodynamics of the jet development from these burners. Computational Fluid Dynamics (CFD) is an effective tool to investigate aerodynamics of the burners, and this paper presents the results of CFD simulations of several slot-burner models based on real geometries used in coal-fired power stations in Victoria. The CFD software CFX-5 has been used for this study. The effect of the primary to secondary jet velocity ratio for different burner geometries has been investigated and the validation of the numerical results has been carried out by comparison with the available measured data.

NOMENCLATURE

C constant
K turbulent kinetic energy
S source or sink term
U fluid velocity
ε dissipation rate
Γ diffusion coefficient
λ jet velocity ratio
μ molecular viscosity
μ_T turbulent viscosity
ρ density
σ turbulent prandtl number

INTRODUCTION

Victoria's Latrobe Valley brown coal deposit is unique due to its high moisture content. To minimize furnace fouling and pollutant production and to ensure optimum combustion stability and efficiency when burning this fuel it is necessary to obtain an improved understanding of the relevant combustion and heat transfer processes. Combustion in a coal fired power station boiler can be divided into two parts: ignition and early combustion of the pulverized fuel, which is controlled by the burner and overall combustion and heat transfer which is controlled by the furnace environment. Although a number of extensive studies of swirl burner design and operation have been undertaken (Johnson et al, 1976 and Pleasance, 1980) a comprehensive study of the operation and basis for optimization of slot burners for tangentially-fired boilers is yet to appear in the open literature. In 1981 a research program was initiated to investigate the aerodynamics of a slot burner system. This was seen as the first step towards including details of fluid flow in a general descriptive model of the ignition and early combustion processes in the burner. A review of the available literature (Perry,1982) revealed little information directly relevant to the rectangular jets. As a result an experimental program was initiated to investigate the influence on isothermal jet development of primary to secondary jet velocity ratio, burner geometry, burner exit velocity profile and fuel particles in the primary stream. During 1981 the flow development and mixing characteristics were measured in a three-jet burner model where the burner face was located at the wall and the jet issued normal to the boiler wall. Perry et al. (1984,1986) conducted some experiments, which investigated the influence of typical secondary to primary jet velocity ratio, burner geometry and burner exit velocity profile on the near field jet development downstream of the model burners. Further research on the effect of particles in the jet stream was performed by Yan and Perry (1994). Four simple burner geometries were characterized including a single near rectangular jet, three jets discharging at right angles to the furnace wall (geometry A), the three-jet system discharging at an angle (60°) to the wall with the jet dividers terminating at the furnace wall (geometry B), the same as geometry B but terminating a short distance upstream of the furnace wall (geometry C) and finally a recessed burner with divergent recess walls (geometry D). Experimental data covers a wide range of secondary to primary jet velocity ratios and includes flow visualization observations and transverse velocity profile and static pressure measurements.

From those experiments Perry concluded that burner geometry can significantly influence the jet development and that the jet velocity ratio can have significant influence with a recessed burner. Perry also concluded that for a typical velocity ratio used in combustion systems, significant deviation of the jets can occur from the geometric centreline and burner exit velocity profile variations can influence the subsequent development of the jet flow field. James et al. (1999) studied in detail three different burner geometries (A, B and D) for jet velocity ratio of 1.0. This paper presents the numerical simulation of rectangular slot burners for different jet velocity ratios. Geometry C and D have been chosen for investigation as recessed burners can play an important

role in the development of the jet. The CFD software CFX-5 has been used in this study. CFX-5 is a coupled solver and uses an unstructured grid. The mathematical model employed to obtain the predictions solves the governing equations for the ensemble-averaged values of the components of the velocity vector, pressure and turbulence parameters. The k-ε model was used for turbulence closure. The results obtained for different jet velocity ratio were validated against the available experimental data.

MODEL DESCRIPTION

The dimensions of the cross section of the primary jet and the secondary jet in the cold flow model are (37.5mm x 29mm) and (37.5mmx17mm) respectively. The hydraulic diameter (D_e) of the jet is 0.0327m. Upstream of the jet, the duct length is 1.95m, which is equivalent to $52D_e$. The jets discharge into the open atmosphere. Due to the symmetry, half of the primary and one full secondary jet has been simulated, which reduced the CPU time and mesh requirement. Very near to the wall the mesh size was 2.8mm and it gradually increased downstream of the furnace wall. The Y plus value was around 45. The secondary jet velocity was kept constant and the primary jet velocity was varied to get the required jet velocity ratio. The results have been investigated for jet velocity ratios (λ) of 1.0, 1.4 and 3.0. The total number of elements used was 1010580.

MATHEMATICAL MODELLING

The general form of the governing equation can be written as

$$\frac{\partial}{\partial x_i}\left(\rho U_i \Phi\right) = \frac{\partial}{\partial x_i}\left(\Gamma \frac{\partial \Phi}{\partial x_i}\right) + S_\Phi \qquad (1)$$

where ρ, U and Γ are the density, velocity and the diffusion coefficients. This equation describes the local change of the variable Φ due to convection, diffusion and production under steady state conditions. Depending on Φ, the above equation represents mass, momentum or turbulence quantities. The k-ε turbulence model was used in this study. This model solves two transport equations for turbulent kinetic energy and eddy dissipation rate. The two transport equations are

$$\nabla.\left(\rho U k\right) - \nabla.\left(\mu + \frac{\mu_T}{\sigma_k}\right)\nabla k = P + G - \rho\varepsilon \qquad (2)$$

$$\nabla.\left(\rho U \varepsilon\right) - \nabla.\left(\left(\mu + \frac{\mu_T}{\sigma_\varepsilon}\right)\nabla \varepsilon\right) = C_1 \frac{\varepsilon}{k}\left(P + C_3 \max\left(G,0\right)\right) - C_2 \rho \frac{\varepsilon^2}{k} \qquad (3)$$

A second order discretization scheme was selected for the convection terms in the k-ε model.

RESULTS AND DISCUSSION

The results obtained are discussed in the following section and compared with the available experimental data (Perry and Hausler, 1984) where possible. Figure 1(a) shows the velocity decay of the primary and secondary jet in geometry D for a jet velocity ratio of 1.0 along the geometric axis. At the exit of the burner the decay rate both for primary and secondary jet were slow up to X/D_e =3 and then increased rapidly further downstream. Initially this decay was due to momentum diffusion within and close to the cavity resulting from the expansion in both primary and secondary jets. Further downstream the decay occurred due to entrainment into the primary jet from its surroundings.

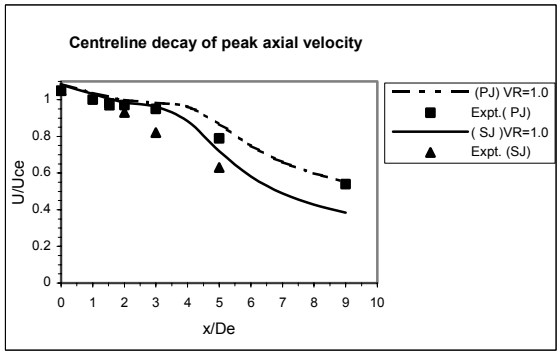

Figure 1(a): Centreline decay of peak axial velocity for primary and secondary jet (geo D, λ=1.0).

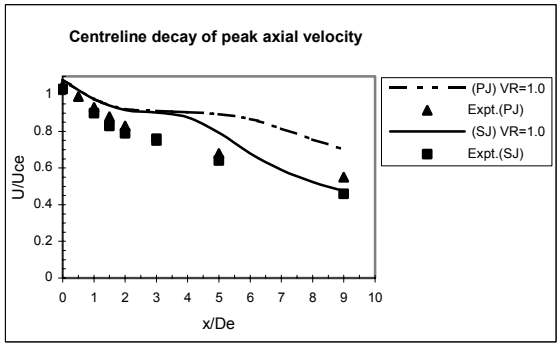

Figure 1(b): Centreline decay of peak axial velocity for primary and secondary jet (geo C, λ=1.0).

The secondary jet decayed faster than the primary. All velocities have been normalized with the centreline velocity at the exit of the burner of geometry A to compare the numerical results with experimental values. The velocity for geometry D at the burner mouth was significantly higher due to low static pressure compared to geometry A. That's why for geometry D, at the exit of the burner the normalized velocities both for primary and secondary jet were higher than 1.0. The predicted decay rate for the primary jet matched reasonably with the experimental results. Although the predicted secondary jet decay rate slightly deviated from the experimental results, the trend was similar i.e. decayed faster than the primary jet. Similar behaviour was observed for burner geometry C, which is clear from fig. 1(b).

Figure 2(a) shows the comparison of primary jet decay rate between geometry C and D for λ= 1.0. For geometry D and λ=1.0, the initial decay rate of the primary jet is much slower than that observed for geometry C due to the reduced cavity diffusion rate. Although the experimental values at X/D_e =9 for geometry C and D are same, the numerical results under predicted the decay rate for geometry C. The experimental values for geometry D matched reasonably well with the predicted results. Figure 2(b) and 2(c) show the primary jet decay rate for geometry C and D respectively for different jet velocity ratio. For geometry C and λ=1.4, the decay rate increased within and downstream of the cavity. For λ=3.0, the peak

centreline value began to increase with increasing X/D_e beyond X/D_e=5. This was attributed to the two secondary jets mixing across the whole of the primary field and increasing fluid momentum in this region. In figure 2(c), with increasing λ, the primary jet decay rate increased both within and downstream of the cavity and for λ=3.0, the primary jet disappeared around X/D_e =4.5.

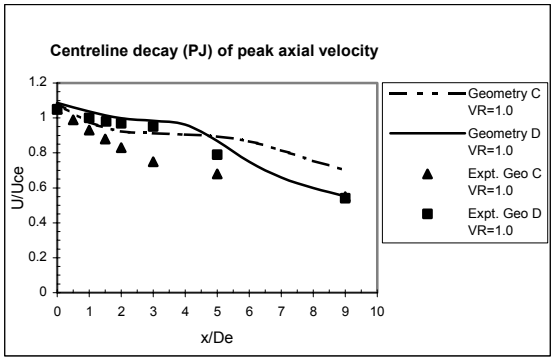

Figure 2(a): Comparison of centreline decay of the primary jet between geometry C and D (λ=1.0).

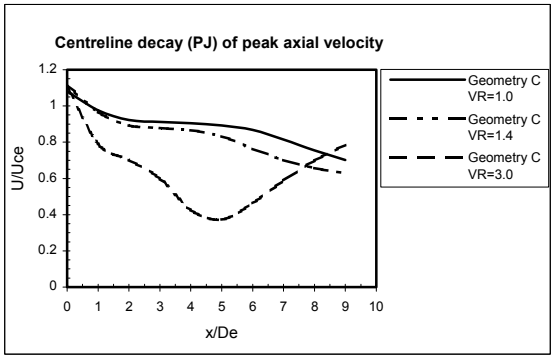

Figure 2(b): The effect of jet velocity ratio on primary jet for geometry C.

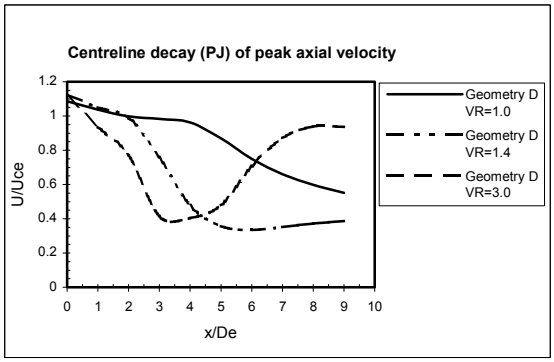

Figure 2(c): The effect of jet velocity ratio on primary jet for geometry D.

This phenomenon can be understood more clearly with the help of figures 3(a) and 3(b), which have been described in the next section. As with trends observed for geometry C, the secondary jets mixed across the primary field beyond X/D_e=5 producing a progressively increased momentum in this region.

Figures 3(a) and 3(b) show the shaded velocity contours for the primary jet (λ=3.0) at the centreline in the xy plane for geometry C and D respectively. For geometry D, the primary jet diverged strongly away from the geometric axis towards the long wall of the cavity. The jet then penetrated up to X/D_e=4. There is a region between X/D_e=3 to X/D_e=4.5 where the primary jet apparently disappeared and after that from X/D_e=5, it became prominent again because of the mixing of the secondary jets. For geometry C the jet diverged significantly but the deviation was not as much as it was for geometry D.

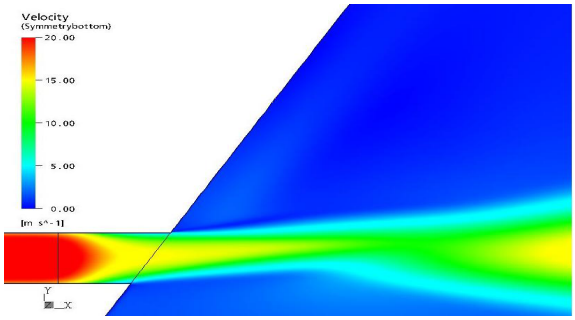

Figure 3(a): Velocity contour at the centreline in the xy plane for geometry C.

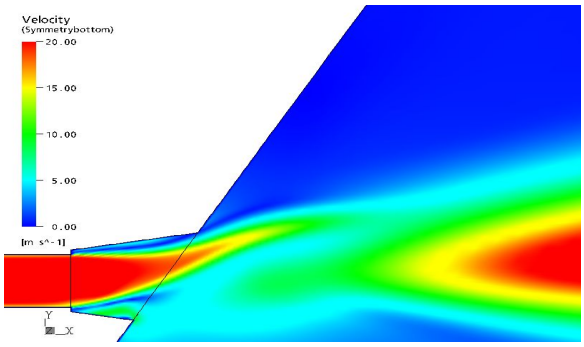

Figure 3(b): Velocity contour at the centreline in the xy plane for geometry D.

Transverse velocity profiles for geometry D in the xy plane through the centre of the primary jet for λ=1.0,1.4 and 3.0 are shown in figures 4(a), 4(b) and 4(c) respectively and compared with the experimental results where possible. Velocity profiles for geometry D (λ=1.0), figure 4(a), shows that generally the behaviour of the predicted jet is same as observed in the measured jet. However there are some deviations between the predicted results and the experimental values. At one hydraulic diameter the peak value of the calculated jet was well matched with the experimental results but the boundaries were a little wider both on the long and short wall side than the measurements indicated. At five diameters the predicted values on the long wall side matched well but the measured profile had a lower peak velocity in the centre of the jet and the boundary was thinner on the short wall side. There is a clear indication of the deviation of the jet towards the long wall side at this position although the measured jet deviated more than the predicted jet across the geometric axis.

At nine diameters the experimental jet had deviated even more from the geometric axis and the profile had become wider than at five diameters. The predicted jet moved further off from the geometric axis and the peak velocity also reduced but not enough to match the experimental jet. With the increase of jet velocity ratio from 1 to 1.4 the behaviour of the jets remain unchanged except the deviation across the geometric axis. Figure 4(b) shows the transverse velocity profile for jet velocity ratio 1.4. At five diameters the deviation across the geometric axis both for predicted and measured values are more than that of

λ=1.0. This can be understood more clearly at nine diameters where the deviation of the peak values of the predicted results for λ=1.4 and λ=1.0 are 1.1m and 0.55 m respectively.

For λ=3.0, the jet started deviating just after the exit of the burner mouth and the deviation is 0.2 m at one diameter as shown in figure 4(c). This trend continued with the increase of the distance and at X/D_e=4.5, the jet apparently disappeared which has been discussed before.

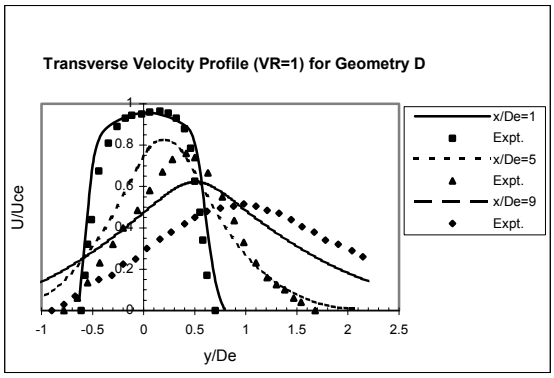

Figure 4(a): Transverse velocity profiles for jet velocity ratio 1.0 (geometry D).

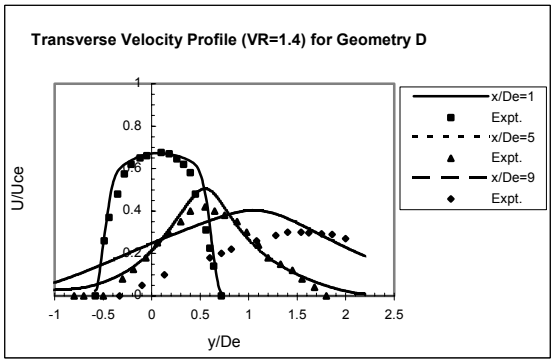

Figure 4(b): Transverse velocity profiles for jet velocity ratio 1.4 (geometry D).

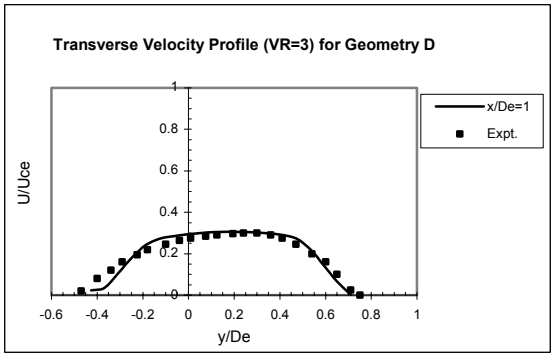

Figure 4(c): Transverse velocity profile for jet velocity ratio 3.0 (geometry D).

Figures 5(a), 5(b) and 5(c) show the transverse velocity profiles for geometry C in the xy plane through the centre of the primary jet for λ=1.0, 1.4 and 3.0 respectively. For λ=1.0, figure 5(a), the predicted jet and the experimental jet showed a similar behaviour. The peak value in the centre line of the geometric axis was over predicted at five and nine diameters. At nine diameters the predicted jet deviated from the geometric axis, whereas the peak value for the experimental jet was along the geometric axis. With the increase of the jet velocity ratio, figure 5(b), the jet deviated towards the long wall side similar to geometry D but the deviation was not as much as it was in geometry D. For λ=3.0, figure 5(c), the deviation was more than λ=1.4. In figure 5(c) the deviation at nine diameters was less than at five diameters because of the increased momentum resulting from the mixing of the secondary jets with the primary jet.

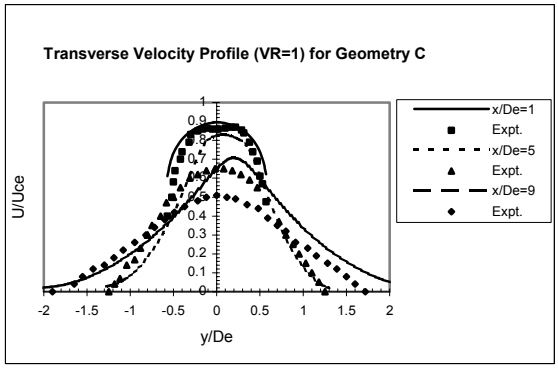

Figure 5(a): Transverse velocity profiles for jet velocity ratio 1.0 (geometry C).

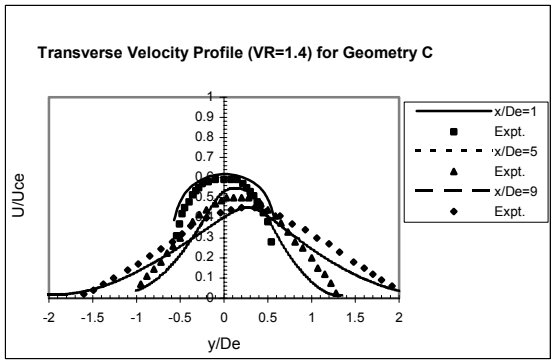

Figure 5(b): Transverse velocity profiles for jet velocity ratio 1.4 (geometry C).

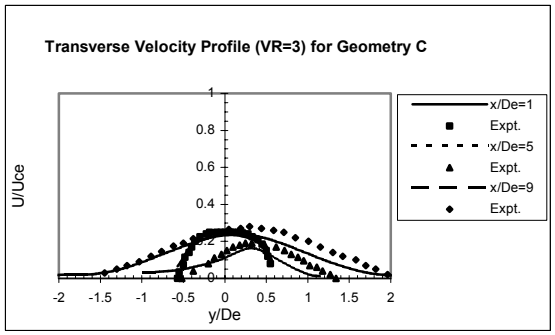

Figure 5(c): Transverse velocity profiles for jet velocity ratio 3.0 (geometry C).

Figures 6(a) and 6(b) show the deviation of the jet centre away from the geometric axis for geometry C and D. The deviation has been measured by considering the distance of peak velocity from the geometric axis at various hydraulic diameters downstream of the furnace wall. With the increase of jet velocity ratio the deviation increased both for geometry C and D. However for λ=3.0, the deviation at x/De=9 was less than x/De=5 both for geometry C and D. The deviation for geometry D was more than geometry C for the same jet velocity ratio. The comparisons between the predicted results and the

measured values for geometry C and D for λ=3.0 are shown in figures 6(c) and 6(d). In figure 6(c) the values were well matched near to the wall up to x/De=1.5. With increased distance the numerical results under predicted the jet displacement and the difference was largest at x/De=9. For geometry D, figure 6(d), the predicted results for the deviation were very well matched up to x/De=4 and after that the numerical results were under predicted like geometry C.

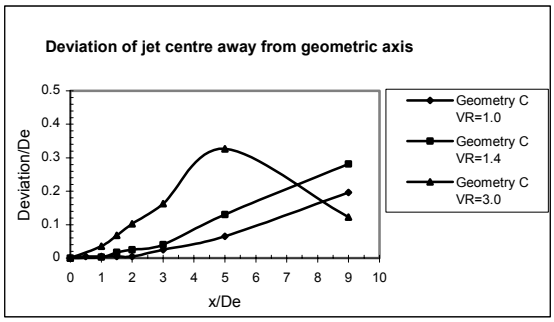

Figure 6(a): Deviation of jet centre with the increase of jet velocity ratio for Geometry C

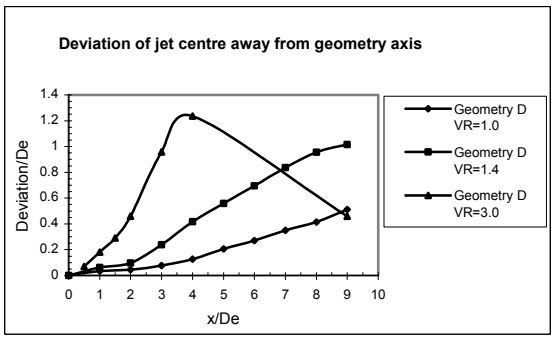

Figure 6(b): Deviation of jet centre with the increase of jet velocity ratio for Geometry D

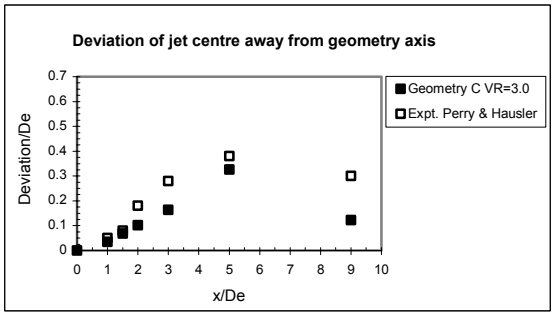

Figure 6(c): Validation of the predicted jet deviation with the experimental values for geometry C (λ=3.0).

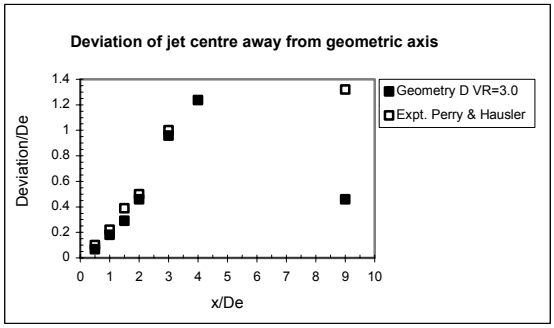

Figure 6(d): Validation of the predicted jet deviation with the experimental values for geometry D (λ=3.0).

Figures 7(a-c) show the velocity vectors for geometry D in the xy plane through the centre of the primary jet for λ=1.0, 1.4 and 3.0 respectively. In figure 7(a), the primary jet separated completely from the short wall whereas it is neither completely attached nor separated from the long wall, consistent with the observations of Perry and Hausler (1982). The separation of the primary jet from the short wall resulted in entrainment of fluid into the recess on that side.

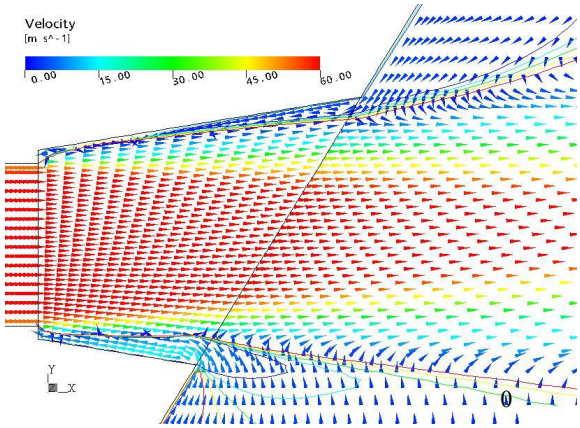

Figure 7(a): Velocity vector for geometry D through the centre of the primary jet for λ=1.0.

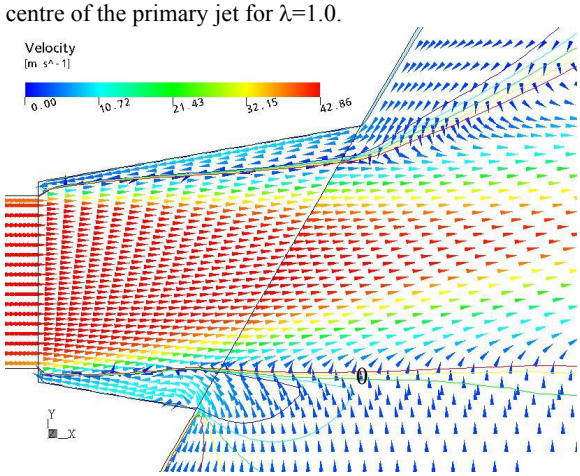

Figure 7(b): Velocity vector for geometry D through the centre of the primary jet for λ=1.4.

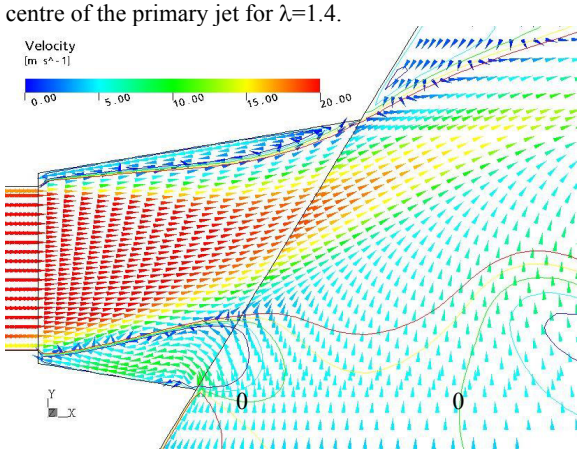

Figure 7(c): Velocity vector for geometry D through the centre of the primary jet for λ=3.0.

Because of the partial attachment to the long wall and separation from the short wall the jet pushed off from the geometric axis towards the long wall side. With the increase of the jet velocity ratio, λ=1.4 and 3.0, the

primary jet completely separated form the long wall and the thickness of separation from the short wall was increased resulting in more deviation of the jet from geometric axis.

CONCLUSIONS

A numerical investigation of the recessed burners has shown that burner geometry and jet velocity ratio can significantly influence jet development. Comparisons have been drawn between the numerical results with the experimental data and reasonably good agreement was found. For a burner geometry where the cavity has parallel sidewalls (geometry C), the primary jet expands along the geometric axis of the burner when the secondary to primary jet velocity is unity but tends to move away from this axis towards the long face of the cavity when the velocity ratio was increased. By replacing the parallel walls in the cavity by diverging walls (geometry D) the centreline decay rate within the cavity was reduced due to a reduced cavity diffusion rate but increased rapidly some distance downstream as it discharged into the furnace. The primary jet deflected strongly towards the long face of the cavity for all velocity ratios. The degree of deflection of the primary jet increased with velocity ratio. For a jet velocity ratio of 3.0, the primary jet apparently disappeared at around four and a half diameters downstream of the jet exit and became very unstable. This numerical investigation indicates that simple small-scale isothermal models can be a major aid in the interpretation of observations in more complex flow environments.

ACKNOLEDGEMENTS

The authors gratefully acknowledge the financial and other support received for this research from the Cooperative Research Centre (CRC) for Clean Power from Lignite, which is established and supported under the Australian Government's Cooperative Research Centres program.

REFERENCES

HART J., NASER J., WITT P., MITTONI L., (1999), "Numerical Modelling of Isothermal Burner Jets", *Second International Conference on CFD in the Minerals and Process Industries,* CSIRO, Melbourne, Australia, 1999.

JOHNSON T R., MORLEY W J., THOMAS GR., (1976), " Firing of Raw Brown coal using Swirl Burners in a Power Station Boiler", *4th Nat. Conf. On Chem. Eng.,* I E Aust, Adelaide, 1976.

PERRY J.H., (1982), ''Aerodynamics of Burner Jets Designed for Brown-Coal Fired Boilers – Part I Literature Survey'', *SECV Engineering Research Division Report No G0/82/53*, 1982.

PERRY J.H., HAUSLER T., (1982), " Aerodynamics of burner jets designed for brown-coal fired boilers – part III', *SECV Engineering Research Division Report No GO/83/57,* December, 1982.

PERRY J.H., HAUSLER T., (1984), "Aerodynamics of Burner Jets Designed for Brown-Coal Fired Boilers – Part-IV", *SECV Engineering Research Division Report No ND/84/004,* March, 1984.

PERRY J.H., SOMOGYI M., REZK M., (1986), "Aerodynamics of Burner Jets Designed for Brown-Coal Fired Boilers–Part-V", *SECV Engineering Research Division Report No ND/86/029,* August, (1986).

PLEASANCE G., (1980), ''Self-Induced Recirculation Characteristics of a Swirl Burner'', *7th Aust. Hyd. and Fluid Mech. Conf.,* August, 1980.

YAN H., PERRY J.H., (1994),"Two–Phase Flow Development in Slot Burners - Part 2 Detailed Flow Measurement and Numerical Model Validation", *ESAA Report No. ES/94/01*, August, 1994.